Optical Reflectivity and Raman Scattering in Few-Layer-Thick Graphene Highly Doped by K and Rb.

Naeyoung Jung,*,† Bumjung Kim,† Andrew C. Crowther,† Namdong Kim,‡ Colin Nuckolls,† and Louis Brus†

†Department of Chemistry, Columbia University, New York, New York, 10027, and ‡Center for Superfunctional Materials, Department of Chemistry and Department of Physics, Pohang University of Science and Technology, Pohang 790-784, Korea

ABSTRACT We report the optical reflectivity and Raman scattering of few layer (*L*) graphene exposed to K and Rb vapors. Samples many tens of layers thick show the reflectivity and Raman spectra of the stage 1 bulk alkali intercalation compounds (GICs) KC_8 and RbC_8. However, these bulk optical and Raman properties only begin to appear in samples more than about 15 graphene layers thick. The 1 L to 4 L alkali exposed graphene Raman spectra are profoundly different than the Breit–Wigner–Fano (BWF) spectra of the bulk stage 1 compounds. Samples less than 10 layers thick show Drude-like plasma edge reflectivity dip in the visible; alkali exposed few layer graphenes are significantly more transparent than intrinsic graphene. Simulations show the in-plane free electron density is lower than in the bulk stage 1 GICs. In few layer graphenes, alkalis both intercalate between layers and adsorb on the graphene surfaces. Charge transfer electrically dopes the graphene sheets to densities near and above 10^{+14} electrons/cm^2. New intrinsic Raman modes at 1128 and 1264 cm^{-1} are activated by in-plane graphene zone folding caused by strongly interacting, locally crystalline alkali adlayers. The K Raman spectra are independent of thickness for $L = 1$–4, indicating that charge transfer from adsorbed and intercalated K layers are similar. The Raman G mode is downshifted and significantly broadened from intrinsic graphene. In contrast, the Rb spectra vary strongly with *L* and show increased doping by intercalated alkali as *L* increases. Rb adlayers appear to be disordered liquids, while intercalated layers are locally crystalline solids. A significant intramolecular G mode electronic resonance Raman enhancement is observed in K exposed graphene, as compared with intrinsic graphene.

KEYWORDS: graphene · alkali · reflectivity · K · Rb · contrast · Raman · intercalation · doping · Drude · superlattice

Both single layer graphene and bulk graphite are semimetals with a low density of states at the intrinsic Fermi level, and relatively few metallic electron carriers. Both show continuous featureless ("gray") electronic spectra across the visible and IR. Generally speaking, in such "metallic" systems without a HOMO–LUMO gap, the molecular Born–Oppenheimer separation of electronic and vibrational degrees of freedom can be a poor approximation.[1] One experimental consequence in graphene is nonadiabatic vibronic (electron–phonon) coupling of the 1580 cm^{-1} aromatic carbon stretching G vibration to the continuum of in-plane-polarized π electron optical transitions. This interaction influences the G mode Raman frequency, and creates a 10 cm^{-1} G phonon lifetime broadening due to decay into isoenergetic metallic electron–hole pairs, as originally observed in graphene Raman spectra by Ferrari and co-workers.[2] Graphene can be modestly charged in gated field effect devices.[3,4] Electron charging moves the Fermi level up to a position of higher π^* state density, changes the π electron optical spectrum, and thus modifies the vibronic coupling. At a doping near 5.5×10^{12} electrons/cm^2, the Fermi level shifts by 0.3 eV; this is accompanied by a *ca.* 10 cm^{-1} frequency upshift and narrowing of the G band. Bulk graphite intercalation compounds (GICs) can exhibit far larger Fermi level shifts and electron–phonon coupling due to charge transfer onto the graphene sheets.[5] In the extreme case of the stage 1 alkali metal intercalated graphites KC_8, and RbC_8, which have a dense atomic metal layer between every graphene layer, the Fermi level shifts are 1.35 eV and 1.6 eV correspondingly, with a graphene-free electron density approaching 5×10^{14} cm^{-2}. This extreme electron doping produces major changes in graphite electronic and optical properties. The optical spectrum shows a Drude-like optical plasma edge and reflectivity dip; stage 1 alkali metal intercalated graphite appears gold to the eye. The G band Raman spectrum shows an asymmetric Breit–Wigner–Fano (BWF) line shape downshifted to 1522 cm^{-1} with a lifetime broadening of about 150 cm^{-1}. In nonadiabatic electronic structure theory, the G Raman mode reversal from upshift to downshift occurs near 10^{+14} electrons/cm^2 as the graphene lattice constant lengthens at high antibonding π^* electron density.[6,7] One measure of this extreme electron–phonon coupling in KC_8 is the 311 cm^{-1} difference between the calculated adiabatic and nonadiabatic G phonon frequencies;

* Address correspondence to nj2153@columbia.edu.

Received for review April 14, 2011 and accepted June 19, 2011.

Published online June 19, 2011
10.1021/nn201368g

this difference is apparently the largest known for any material.[5] This strong coupling of the G mode is also directly observed in ARPES photoemission studies.[8,9]

In this paper we explore how the nonadiabatic electronic properties of alkali doped bulk graphite develop in few layer thick intercalated graphenes, as a function of the number of layers L, starting from a single graphene layer with adsorbed alkali atoms. We study both optical reflectivity and Raman scattering, as they reveal different aspects of the electronic structure. Note there are also recent Raman studies of intercalation by $FeCl_3$,[10,11] sulfuric acid,[12] and bromine[13,14] in few-layer-thick graphenes.

RESULTS

Optical Reflectance. Optical reflectivity is a direct measure of electronic response.[15−17] As a model for simulations, we use the known optical dielectric constants of graphene and of the bulk alkali metal compounds which are identical for KC_8 and RbC_8 and initially assume them to be independent of sample thickness. This approach works well for the reflectivity of undoped few layer graphenes as a function of thickness.[18] From the dielectric constant we simulate the measured data: contrast $(\omega) = (R_{g+s} - R_s)/R_s$ and reflectance $(\omega) = R_{g+s}/R_M$. Here, R_{g+s} is the reflected light from graphene on substrate, R_s is the reflected light from a nearby spot on the bare substrate, and R_M is the reflected light from a perfect mirror. In the limit of a thin film, contrast is directly proportional to optical absorption *via* the relation[19]

$$\text{contrast}(\omega) = \frac{R_{g+s} - R_s}{R_s} = \frac{4}{{n_s}^2 - 1} A$$

where n_s is the quartz substrate index of refraction and A is the thin film absorbance. We calculate reflectance and contrast as a function of L using Fresnel interference equations as described recently.[14] Figure 1 shows experimental and simulated small L contrast data before graphene exposure to alkali vapor. As previously reported the simulations using the graphene optical dielectric constant are close to the data in both shape and magnitude. Small differences create a ± 1 layer uncertainty above approximately 10 L for use of contrast to determine thickness.

The reported bulk stage 1 alkali metal intercalated graphite dielectric constant in the visible and IR is well fit by a Drude free carrier model with $\varepsilon_\infty = 8$, dimensionless plasma frequency $\omega_p = 6.6$, and mean carrier lifetime $\tau_D = 19/\omega_p$.[20] In this approximation, neglecting the additional interband π to π^* optical absorption term,[21] the alkali metal intercalated graphite dielectric function $\varepsilon(\omega) = \varepsilon_\infty - {\omega_p}^2/(\omega(\omega + i/\tau_D))$. Figure 2a shows alkali metal intercalated graphite reflectance simulations for thicknesses up to 500 L on quartz substrate. The thicker L samples show a dip around 2.5 eV in the blue, corresponding to the reflectivity minima at the plasma frequency of bulk intercalated graphite. The increase in reflectance at lower energies is the optical response of the free electrons. Note that the Drude plasma frequency is proportional to the square root of the average volume density of free electrons moving in plane, in both alkali and graphene layers. In stage 2 bulk alkali metal intercalated compounds MC_{24}, with graphene bilayers between metal layers, the free electrons initially in metal layers are diluted over a larger volume, and the reflectivity dip drops to near 1.8 eV.[21]

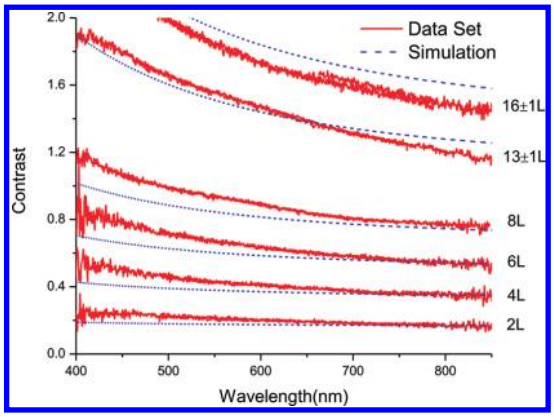

Figure 1. Simulated and experimental contrast for pristine graphene from 2 to 16 ± 1 L.

Our measured "large L" spectrum observed after graphene exposure to alkali metal vapor in Figure 2b is close to our simulation for L = 100 or 500. This result confirms that upon exposing our samples to alkali metal vapor, we actually make stage 1 intercalated graphite. Actually the plasma frequency in our sample is slightly (0.1 eV) above the reported bulk frequency. At energies above the plasma frequency, where the Drude reflectance is very weak, the 100 and 500 L simulations shows an oscillation pattern due to internal reflection within the thin film. Under our experimental conditions, we do not detect such an interference pattern above 3.1 eV (under 400 nm). If the interband π to π^* dielectric term were included, the extra absorption in this region would likely damp these oscillations. Note that Figure 2a should apply to all alkali stage 1 GICs as the reported bulk optical dielectric constants fits are very similar.

In Figure 3 the few-layer graphene contrast data upon exposure to K and Rb vapors are significantly weaker compared with undoped graphenes in Figure 1. The data show a Drude-type response with a pronounced reflectivity dip near 510 nm (2.43 eV). Figure 4 compares the 16 ± 1 L K data with simulations based upon both stage 1 and stage 2 bulk dielectric constants. The data run significantly below the stage 1 simulation, and higher than stage 2. A 15% reduction in the stage 1 plasma frequency fits the rising free electron response in the red. This intermediate result is generally valid for all L for both K and Rb. Figure 5 shows in greater detail the 2 L contrast data before and

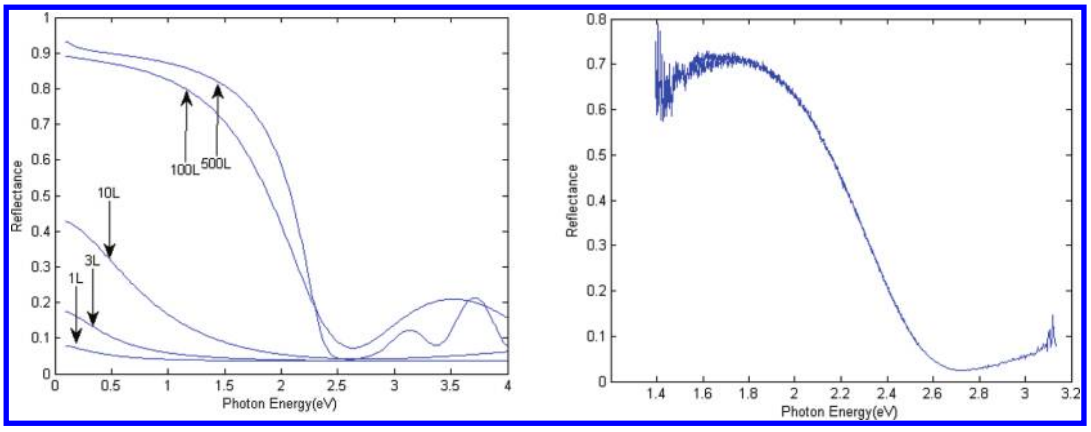

Figure 2. (a) Reflectance simulation for stage 1 alkali metal intercalated graphene as a function of *L* from 1 to 500 L. (b) Experimental reflectance of "thick" potassium intercalated graphite flake.

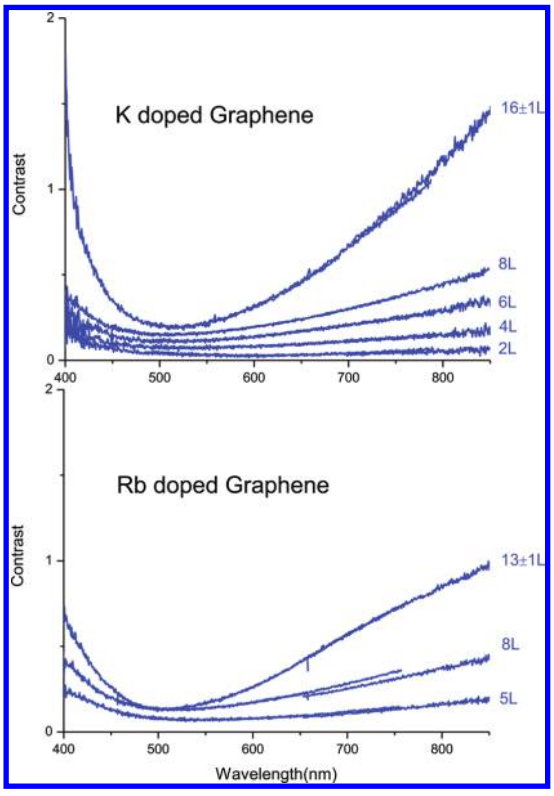

Figure 3. (a) Experimental contrast for potassium-doped graphene 2 to 16 ± 1 L; (b) experimental contrast for rubidium-doped graphene 5 to 13 ± 1 L. The data are composed of overlapping sections from different spectral regions.

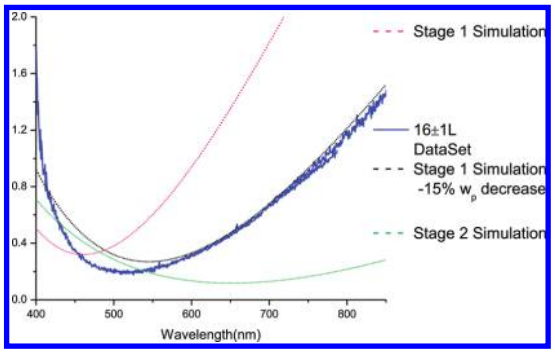

Figure 4. (Blue data) 16 ± 1 L potassium-doped graphene contrast; (pink dotted line) stage 1 contrast simulation (ε_∞ = 8, ω_p = 6.6, $\tau_D\omega_p$ = 19); (green dotted line) stage 2 contrast simulation (ε_∞ = 7, ω_p = 4.2, $\tau_D\omega_p$ = 22); (black dotted line) 15% reduced plasma frequency simulation from stage 1 (ε_∞ = 8, ω_p = 5.61, $\tau_D\omega_p$ = 19).

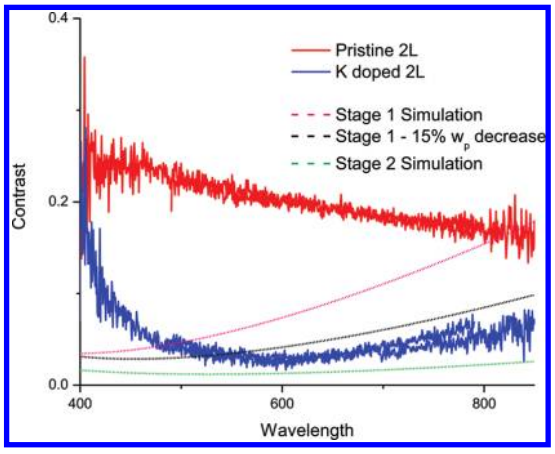

Figure 5. (Blue data) 2 L potassium-doped graphene contrast; (red data) 2 L pristine graphene contrast; (pink dotted line) stage 1 contrast simulation (ε_∞ = 8, ω_p = 6.6, $\tau_D\omega_p$ = 19); (green dotted line) stage 2 contrast simulation (ε_∞ = 7, ω_p = 4.2, $\tau_D\omega_p$ = 22); (black dotted line) 15% less plasma frequency simulation from stage 1 (ε_∞ = 8, ω_p = 5.61, $\tau_D\omega_p$ = 19).

after exposure to K vapor. The reflectivity dip has shifted red from 510 nm at larger *L* to about 600 nm, indicating a slight further lowering of the average free electron density. The contrast on quartz substrates is so weak that we could not optically locate single layer graphene samples after exposure to alkali.

The data show increased contrast below 500 nm compared with the stage 1 and stage 2 simulations, apparently due to the missing interband contribution in the simulation. In addition our simulation does not correctly account for both adsorbed (top and bottom) metallic monolayers. For example the 2 L sample has one intercalated metal layer and two adsorbed metal

layers. The 2 L simulation film thickness is twice the repeat distance of stage 1 KC_8; this effectively incorporates one adsorbed layer only. Furthermore, there could be adsorbed metal layers more than one monolayer thick, as the samples are exposed to excess alkali during synthesis at high temperature. We calculated the effect of a K metal adlayer of variable thickness on top of the intercalated graphene small *L* sample by modification of the Fresnel equations; this simulation uses the dielectric constant of bulk K metal. In general, if we assume a 5 nm thick metallic K layer on top of a sample, then the simulated contrast of the combined system is larger than that of the sample without the K adlayer (result not shown). We observe a smaller contrast than expected for stage 1 KC_8 samples; this result is not due to a K metal overlayer on stage 1. In our samples we have a lower density of free electrons than present in bulk stage 1.

The contrast measurements were performed with a 40×/0.6 N.A. microscope objective. The objective numerical aperture influences Rayleigh contrast measurements of graphene on a silicon substrate containing a dielectric spacer.[16] However, including these effects in the simulation of previous contrast measurements of graphene on quartz changed the results by ~1%, and different objectives yielded the same results experimentally, so we assume only normal incidence here. Furthermore, at the long wavelength limit of the contrast measurements shown in Figure 1, converting the contrast value to absorption yields an absorption per layer of 2.3%, as expected.[22]

Figure 6 shows 12 L simulations for intrinsic graphite, and for stage 3, stage 2, and stage 1 alkali metal intercalated graphite, in the order of increasing free electron density. Each sample contains 12 layers of graphene; the total film thickness depends upon the stage. The thickness is 12 repeat units of stage 1, 6 units of stage 2, and 4 units of stage 3. The contrast difference between stage 1 and stage 2 is pronounced in the visible, and stage 2 is approaching transparency. Our small *L* data are between stage 1 and 2, while the thick sample in Figure 2 shows stage 1 reflectivity.

Raman Scattering. Before alkali exposure, the low *L* graphene Raman spectra[2] do not show a defect D band, indicating their high initial quality. The D band position in graphitic carbon is 1345 cm^{-1} for 514 nm excitation. Figures 7 and 8 show our Raman spectra for K exposed graphenes in the G mode spectra region. For both alkalis at large *L* we observed a severely asymmetrically broadened BWF line shape downshifted from 1580 cm^{-1} to about 1450 cm^{-1}, in agreement with literature Raman spectra for the bulk stage 1 GICs.[23−26] In the modern KC_8 literature, this downshift and extreme broadening (*ca.* 150 cm^{-1}) are attributed to coupling between the continuum of metallic electron−hole states and the discrete phonon G mode state (E_{2g} mode, in plane carbon−carbon stretching), in the presence of high Drude π^* free electron density and Fermi level shift on the graphene sheets. This high

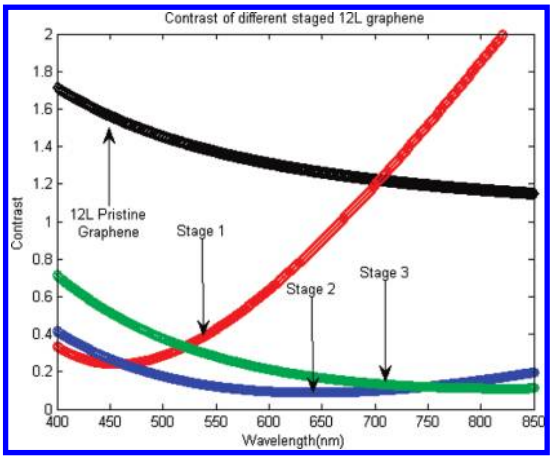

Figure 6. Simulated contrast of 12 L graphene: (black line) 12 L pristine graphene; (red line) 12 units of stage 1 graphene; (blue line) 6 units of stage 2 graphene; (green line) 4 units of stage 3 graphene.

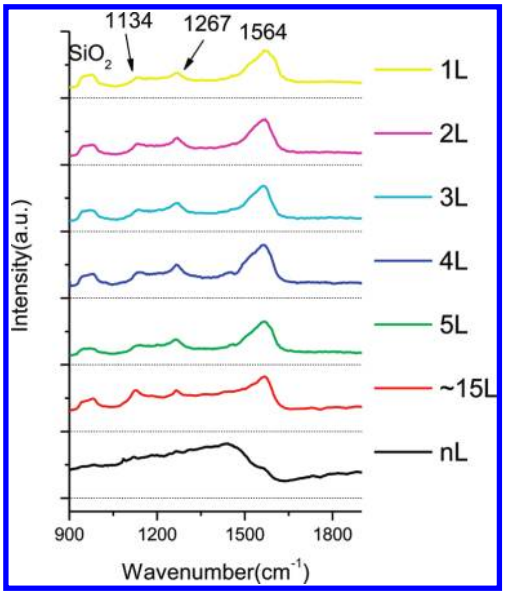

Figure 7. The Raman spectra of potassium exposed graphene as a function of *L*.

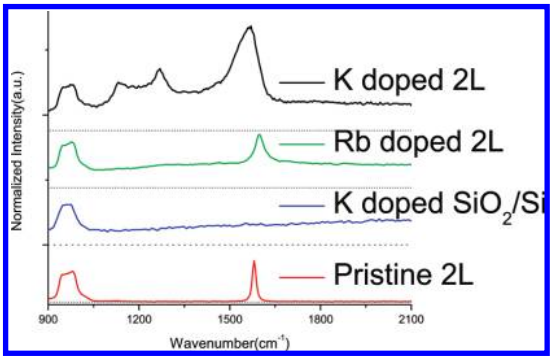

Figure 8. The Raman spectra of 2 L potassium intercalated and rubidium intercalated graphene compared to 2 L pristine graphene, and to the bare substrate exposed to K.

coupling is also directly observed in recent APRES photoemission data.[8,9] The asymmetric BWF line shape equation is

$$I(\omega) = \frac{I_0\left[1+\left(\frac{\omega-\omega_0}{q\Gamma}\right)\right]^2}{\left[1+\left(\frac{\omega-\omega_0}{\Gamma}\right)^2\right]}$$

Where $1/q$ is the coupling constant between continuum states and discrete state, and ω_o is the central frequency; γ is a measure of the broadening. Similar BWF shapes are also observed in other metallic graphitic carbon systems including the lower-frequency G peak in metallic carbon nanotubes[27,28] and the tangential G-band of alkali metal doped carbon nanotube.[29]

As L decreases the Raman spectra change profoundly. For K the strongly asymmetric G peak narrows and shifts upward to 1564 cm^{-1}. The asymmetric G peak figure is almost identical for 1−5 L graphene with a fitted q value as −5 compared to −0.8 in bulk graphite value,[24] indicating less coupling between discrete G phonon and continuum electronic band. Two new Raman modes appear at 1134 and 1267 cm^{-1}. Most remarkably, this novel spectrum does not vary significantly with thickness in the range L = 1−5. In the neighborhood of ∼15 L the spectrum begins to evolve toward the bulk spectrum. These K spectra are very different than all of the higher stage bulk K GIC Raman spectra. This difference proves that K is intercalating between the layers in our low L samples. If K were only adsorbed on graphene for small L, then we would see narrow upshifted G band spectra for those graphene sheets not in direct contact with K layers, as observed in the higher stage K bulk GIC Raman spectra.

The Raman peak near 950 cm^{-1} from the underlying Si substrate is observed when the laser is transmitted through low L graphenes. Figure 8 compares the alkali exposed and intrinsic graphene 2 L Raman spectra; here the 950 cm^{-1} SiO_2/Si substrate line is normalized to serve as an internal intensity standard. The K spectrum is significantly more intense than the intrinsic graphene spectrum. A "control" Raman spectrum of a bare spot on the silica covered wafer shows that strong continuum scattering is observed after bare silica exposure to alkali. This continuum also appears in the low L graphene spectra in Figures 7−9. In the low L graphenes, there appears to be little continuum directly generated by the doped graphenes in comparison with the substrate continuum. In the thick bulk-like BWF spectra, however, there is little penetration of the laser through the sample to the substrate. The bulk asymmetric BWF line shape is understood as interference between an electronic continuum and the discrete G phonon, both generated within the thick sample.

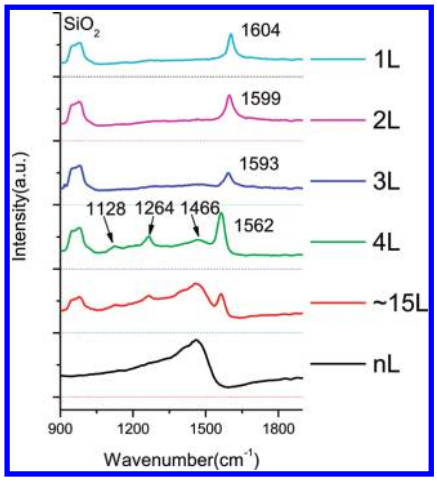

Figure 9. The Raman spectra of rubidium exposed graphene as a function of L.

The Rb exposed Raman spectra in Figures 8 and 9 are different than both the bulk Rb intercalated spectrum, and the thin film K spectra. Moreover, the Rb spectra change strongly in the range L = 1−4, in contrast with the equivalent K spectra. For L = 1∼3 the two new modes at 1128 and 1264 cm^{-1} are absent, yet as thickness increases they grow in intensity and are clearly observed at L = 4. For L = 1 the G mode is a narrow symmetric peak at 1604 cm^{-1}, almost 40 cm^{-1} above the position for K exposed L = 1. For Rb in the range L = 2−4 the G peak broadens and shifts to lower frequency, appearing at 1562 cm^{-1} for L = 4.

DISCUSSION

In both Raman and reflectance experiments the incident optical beam is normal to the graphene sample, with the optical electric field polarized in the plane. The reflectance optical response is determined by the in-plane dielectric constant; we have no direct data on the out of plane dielectric constant as thickness changes. Correspondingly, in our normal incidence, backscattering Raman geometry we observe only in-plane polarized Raman modes. Hexagonal undoped graphene has only one allowed, in-plane polarized Raman mode (the G mode) in our spectra region.

Our reflectance and Raman data for large L alkali-exposed graphene samples agree with published data for bulk stage 1 alkali intercalation compounds. As the alkali-exposed graphene samples become thinner, we observe a pronounced L dependence in the Raman data, while the contrast data show decreased free electron density that varies more gradually with L. Both contrast and Raman data show that many tens of layers are necessary before full stage 1 properties are observed.

The Raman and Reflectivity experiments measure different aspects of the electronic response. Reflectivity measures a volume average free electron density, and has contributions from both π^* electrons on graphene,

and remaining free electrons in the alkali metallic sheets. The averaged free electron density in the bulk stages is primarily sensitive to the ratio between graphene and K free electron layers in the sample. It is less sensitive to whether the Fermi level is primarily in the graphene or K metal sheets. In contrast, the in-plane G Raman spectra and electron−phonon coupling are controlled by the density of in plane free electrons on graphene.[30] This difference can be seen in the stage 3 bulk alkali GICs: The reflectance shows an averaged plasma frequency, while the G mode Raman spectra has contributions from individual graphene planes, one with high and one with low electron doping from the K layers. In the bulk alkali GICs, the strong downshift of the G mode from 1580 cm^{-1} has been explained by the nonadiabatic effect of coupling with π^* electrons.[5,6] The correlation between line width of in-plane phonon mode to the electron phonon coupling strength (phonon decay in electron−hole pairs) is strongly positive.[5] The large line width of the G mode is caused by fast decay into metallic electron−hole pairs.

In field effect devices, single layer graphene is capacitively charged with electrons by the gate potential. The strict hexagonal graphene Raman selection rules are not altered by such charging. However in alkali exposed small *L* graphenes with high in-plane electron densities, we observe new Raman lines at 1134 and 1267 cm^{-1}. These modes are not the damage-related D mode. They are intrinsic graphene modes made Raman active by symmetry lowering due to strongly coupled alkali adlayers. Such superlattice-induced graphene Raman modes have been previously observed in graphite−potassium−amalgam intercalation compounds.[31] Alkali adsorbed and intercalated layers create a p(2 × 2) superlattice structure on graphite.[32] In the graphene Brillouin Zone, the M point is zone-folded back to the Γ point, and thus both Γ and M phonons will be Raman active. Superlattice zone folding shows that our adsorbed and intercalated alkali layers are mostly complete and locally crystalline in our small *L* graphene samples. Hoire *et al*[33] originally calculated the Raman active phonon modes in MC_8 compounds with zone folding, and made possible graphene assignments for the two new modes at 1280 and 1370 cm^{-1}. A modern nonadiabatic Raman calculation[5] with an expanded lattice structure would likely give a closer agreement between experimental and theoretical Raman values.

Charge transfer from K to graphene is stronger than observed in more weakly adsorbed molecular species such as Br_2.[13,14] Substantial charge transfer creates a strong ionic interaction between the alkali and graphene layers, and effectively changes the electrostatic potential seen by the graphene π electrons. In locally crystalline Br_2 adsorbed and intercalated acceptor layers on few *L* graphenes, possible zone folding modes are not observed.

The new Raman modes observed in the K data imply a dense and locally crystalline K adlayer exists on 1 L and 2 L, and interacts strongly with the graphene π electrons. A recent paper reports the 1 L Raman spectra as a function of K coverage in a quartz cell very similar to ours:[34] the observed saturation K spectrum is essentially identical to that in Figure 7. This supports the result that the K adlayers are essentially complete for 1 L and 2 L. Yet we do not observe the full BWF spectrum of bulk KC_8, which develops very slowly with increasing *L*. In addition, as discussed above, throughout this entire range of *L* the contrast data show that the volume density of free electrons in the thin film is lower than that of bulk stage 1 KC_8. In theory[6] a G peak at 1560 cm^{-1} downshifted from the uncharged 1580 cm^{-1} value indicates that the free π^* density on graphene is above 10^{+14} electrons/cm^2, the density must be below the nearly 5 × 10^{+14} electrons/cm^2 value of bulk KC_8. The 1 L Raman spectrum for K shows charge transfer onto graphene from adsorbed layers is important, but not as strong as in the bulk KC_8. The constant spectrum in the range 1−4 L suggests that charge transfer from adsorbed K layers is about the same as from intercalated layers

The K and Rb 1 L Raman spectra are very different. The Rb spectrum does not show zone folding modes and has an upshifted G band, implying less charge transfer than with K. This result might suggest the only a small fractional coverage of Rb on graphene. Yet, the presence of the alkali-induced substrate continuum in both K and Rb spectra is evidence that both samples have been exposed to an excess of alkali. Instead, there is apparently some major difference in the structure of the adlayers. The Rb 1 L spectrum is very close to the stage 2 bulk Rb Raman spectrum which shows a G band of similar width at 1602 cm^{-1}. While the intercalated alkali layer in stage 1 Rb GIC is crystalline p(2 × 2) at 23 C; in stage 2 the metallic Rb layer is a disordered liquid at 23 C, with a lower alkali atom planar density than in stage 1.[35] If the Rb adlayers on 1 L graphene were a disordered liquid X-ray study of the liquid and solid phases of the alkali metals in KC_{24} and RbC_{24}-intercalated graphite single crystals of lower atom density in our experiment, and the K adlayers a locally crystalline p(2 × 2) solid, then this might explain the difference in the 1 L Raman spectra. Disordered liquid adlayers would not induce zone folding.

In comparison with the 1 L spectrum, the 4 L Rb spectrum develops zone folding modes, and shows greater charge transfer with a downshifted G band from 1604 to 1560 cm^{-1}. This observation suggested the intercalated Rb layers in 4 L have a very different structure than the adsorbed layers. The intercalated layers could be closer to the crystalline p(2 × 2) layers of stage 1. Moreover, the ~15 L Rb spectrum in Figure 9 appears to be a sum of the 4 L spectrum and the BWF spectrum of the thick Rb sample. This suggests we might interpret ~15 L as having interior layers yielding a BWF spectrum, and

surface layers yielding spectra like the 4 L spectra. For reference, Fresnel calculations show that about 85% of the Raman signal from bulk KC_8 is generated as the laser penetrates the first 100 layers; thus the broad bulk BWF Raman spectrum is generated many tens of layers deep in the bulk material.

It may be that bulk stage 1 GICs actually have different Raman spectra generated in their top layers close to the surface; this spectrum would be buried under the intense BWF spectrum coming from below. In this regard, the new Raman modes at 1134 and 1267 cm^{-1} we see in the 4 L alkali spectra seem to be washed out by the intense electronic continuum and broad BWF G mode in our thick *n* L spectra. In contrast, these new Raman modes are observed in the bulk $KHgC_8$ amalgam GIC Raman spectrum previously mentioned. The net charge transfer from metal to graphene is thought to be less in the bulk crystalline amalgam compound than in KC_8.[36]

Both Rb and K form p(2 × 2) monolayers when adsorbed on bulk graphite at low temperature,[32] with very little difference in calculated electronic or structural properties.[37] Both show a calculated electron transfer of about 0.1 electron per alkali atom, significantly less than the values typically calculated for the intercalated layers in the stage 1 GICs. Thus it seems reasonable that adsorbed layers on graphene might show less charge transfer than intercalated layers.

Overall, the Raman and contrast data indicate a slow development of the full optical properties of bulk stage 1 GICs with increasing thickness. There may be several factors at work here: First, in small *L* samples exposed to vacuum, the dielectric stabilization of charge transfer should not be as strong as in the high dielectric constant environment that occurs deep in bulk KC_8. Consistent with this idea, adsorbed metals on bulk graphite seem to show less charge transfer than intercalated layers deep in stage 1 GICs. The repeat distance along the Z axis should be longer if metal-to-graphene charge transfer is lower. This would make our small *L* alkali samples actually thicker than we assume in the simulations. A greater film thickness could explain the lower free electron densities that we observe in contrast data. Less interaction with the graphene may create a disordered equilibrium adlayer as we have discussed for Rb.

Second, the development of the full KC_8 delocalization, along the perpendicular *Z* direction may be slow with increasing *L*, even in the region where the intercalated alkali is fully p(2 × 2) crystalline. The π^* band is localized in the graphene plane and shows no dispersion along *Z* in KC_8. However, the Fermi level 1.35 eV above the Dirac point lies partially in the interlayer isotropic band on the K metal.[38] In this regard, note that the *Z* axis electrical conductivity increases from 8.3/ohm-cm in intrinsic graphite to 1.94 × 10^3/ohm-cm in KC_8.[39,40] This increase occurs despite the greater distance between graphene planes in KC_8; current flows through the dense K layers. Recently Boeri *et al*[23] have discussed the *Z* axis spatial dispersion of the interlayer electronic density remaining in the metallic layer, and Gruneis *et al*[8] calculated a close relative spacing of interlayer and π^* bands at the γ point in KC_8. Nevertheless, a quantitative understanding of the KC_8 Fermi level structure, and its development with thickness, require further theoretical work.

In Figure 8 the K 2 L spectrum shows a strong G intensity enhancement with respect to graphene, despite the fact that the K 2 L contrast (and absorbance) at the laser frequency is less than that of intrinsic 2 L graphene. We assign this enhancement to "intramolecular" graphene electronic resonance Raman enhancement, which has previously been observed and recognized in bulk GICs when the laser wavelength is near the π–π^* interband optical gap created by doping.[41–43] There should be no significant electromagnetic field enhancement for few layer graphenes.[14] Note that the G mode Raman downshift and intensity enhancement, and the zone folding activation of new graphene modes, are all larger for K than Rb. This suggests that the π–π^* interband optical gap, caused by charge transfer onto graphene, is larger for K and thus closer to resonance with the 514 nm laser. Yet the contrast reflectivity data are similar for Rb and K few layer samples, again indicating that reflectivity does not directly measure charge transfer.

In conclusion, few layer thick graphenes with intercalated and adsorbed K and Rb layers show a lower free electron density than the corresponding bulk intercalated stage 1 GICs. The Raman spectra indicate less metal to graphene charge transfer than observed for intercalated metals in the bulk GICs, yet new graphene Raman modes are activated by this interaction. Previous nonadiabatic electronic structure Raman theory calculations suggest that few-layer-thick graphenes show free electron densities in the range 5 × 10^{+13} to 5 × 10^{+14} electrons/cm^2 for 4 L and thinner samples; Rb-exposed samples show less charge transfer than K-exposed samples. A BWF Raman spectrum from intercalated interior layers develops as sample thickness increases. Samples ~15 L thick appear to show a superposition of different surface and interior graphene Raman spectra.

METHODS

Single and few layer graphene pieces were deposited by transparent-tape mechanical exfoliation in air onto p-type Si wafer chips with 300 nm thick SiO_2 for Raman measurement and on quartz substrates for reflectivity measurement. The pristine graphene samples were characterized by Raman (on wafers) or contrast (on quartz) to determine the number of layers in each piece for each measurement. Thicknesses determined from contrast measurements on quartz have an uncertainty of ±1 layer. Above five layers, the thickness in Raman measurements on wafers

is more uncertain. Samples about 15 layers thick have a blue color to the eye in the optical microscope; samples we label "thick", with many tens of layers, have a yellow color. Alkali metal exposure was performed in an airtight sealed pyrex or quartz cell initially evacuated to about 2×10^{-5} Torr. Alkali metal was initially cleaned with heptanes and handled under inert argon gas. Cells containing alkali and graphenes samples, both on quartz and on wafers, were heated 5 min at 210 °C for potassium intercalation, and 160 °C for the rubidium intercalation. The calculated alkali pressures at the intercalation temperatures are *ca.* 3 Torr for Rb and 400 Torr for K. The alkali-exposed graphenes were subsequently characterized at room temperature 23 °C in the cell. The cell contained excess alkali metal which effectively eliminates any remaining oxygen and/or water vapor. Raman measurements were performed in the cell using a backscattering geometry. The spot size of the 514.5 nm wavelength beam was $\sim 1\ \mu m^2$ focused using a 40× objective, and the spectral resolution was about 8 cm^{-1}.[42] For contrast and reflection measurements,[43] light from an Oriel quartz tungsten halogen lamp passed through a 100 μm pinhole and was collimated by a $f = 300$ mm achromatic lens doublet. An iris was cut down the diameter of the white light beam to about 2 mm, which was then focused to a 2 μm diameter spot by the microscope. The microscope objective and the spectrometer were the same as for the Raman measurements. We obtained a useful spectral range from about 400 to 850 nm, and we used a holmium perchlorate standard placed in the beam after the microscope to calibrate the spectrum. To avoid intercalate desorption effects associated with laser heating, all the spectra was obtained at the laser intensity of 2 mW for Raman measurement. The spectrum of all the samples we investigated did not change for several hours with 2 mW laser heating without moving the spot. For contrast, white light exposure did not induce any change in optical spectrum for several hours.

Acknowledgment. We thank Irving P. Herman, Tony Heinz, Mark Hybertsen, Chris Marianetti, Michael Steigerwald, Philip Kim, and Zheyuan Chen for productive discussion of this research. We also thank Kin Fai Mak for advice on the contrast measurements. This work has been supported by the AFOSR under MURI FA955009-1-0705. We also acknowledge partial support from the DOE under EFRC Center DE-SC0001085, the Nanoscale Science and Engineering Initiative of the National Science Foundation under NSF CHE-06-41523 and by the New York State Office of Science, Technology, and Academic Research (NYSTAR).

REFERENCES AND NOTES

1. Pisana, S.; Lazzeri, M.; Casiraghi, C.; Novoselov, K. S.; Geim, A. K.; Ferrari, A. C.; Mauri, F. Breakdown of the Adiabatic Born–Oppenheimer Approximation in Graphene. *Nat. Mater.* **2007**, *6*, 198–201.
2. Ferrari, A. C.; Meyer, J. C.; Scardaci, V.; Casiraghi, C.; Lazzeri, M.; Mauri, F.; Piscanec, S.; Jiang, D.; Novoselov, K. S.; Roth, S.; Geim, A. K. Raman Spectrum of Graphene and Graphene Layers. *Phys. Rev. Lett.* **2006**, 97.
3. Das, A.; Pisana, S.; Chakraborty, B.; Piscanec, S.; Saha, S. K.; Waghmare, U. V.; Novoselov, K. S.; Krishnamurthy, H. R.; Geim, A. K.; Ferrari, A. C.; Sood, A. K. Monitoring Dopants by Raman Scattering in an Electrochemically Top-Gated Graphene Transistor. *Nat. Nanotechnol.* **2008**, *3*, 210–215.
4. Das, A.; Chakraborty, B.; Piscanec, S.; Pisana, S.; Sood, A. K.; Ferrari, A. C. Phonon Renormalization in Doped Bilayer Graphene. *Phys. Rev. B* **2009**, 79.
5. Saitta, A. M.; Lazzeri, M.; Calandra, M.; Mauri, F. Giant Nonadiabatic Effects in Layer Metals: Raman Spectra of Intercalated Graphite Explained. *Phys. Rev. Lett.* **2008**, 100.
6. Lazzeri, M.; Mauri, F. Nonadiabatic Kohn Anomaly in a Doped Graphene Monolayer. *Phys. Rev. Lett.* **2006**, 97.
7. Nixon, D. E.; Parry, G. S. The Expansion of the Carbon–Carbon Bond Length in Potassium Graphites. *J. Phys. C: Solid State Phys.* **1969**, *2*, 1732.
8. Gruneis, A.; Attaccalite, C.; Rubio, A.; Vyalikh, D. V.; Molodtsov, S. L.; Fink, J.; Follath, R.; Eberhardt, W.; Buchner, B.; Pichler, T. Angle-Resolved Photoemission Study of the Graphite Intercalation Compound KC_8: A Key to Graphene. *Phys. Rev. B* **2009**, 80.
9. Gruneis, A.; Attaccalite, C.; Rubio, A.; Vyalikh, D. V.; Molodtsov, S. L.; Fink, J.; Follath, R.; Eberhardt, W.; Buchner, B.; Pichler, T. Electronic Structure and Electron-Phonon Coupling of Doped Graphene Layers in KC_8. *Phys. Rev. B* **2009**, 79.
10. Zhan, D.; Sun, L.; Ni, Z. H.; Liu, L.; Fan, X. F.; Wang, Y. Y.; Yu, T.; Lam, Y. M.; Huang, W.; Shen, Z. X. $FeCl_3$-Based Few-Layer Graphene Intercalation Compounds: Single Linear Dispersion Electronic Band Structure and Strong Charge Transfer Doping. *Adv. Funct. Mater.* **2010**, *20*, 3504–3509.
11. Zhao, W.; Tan, P. H.; Liu, J.; Ferrari, A. C. Intercalation of Few-Layer Graphite Flakes with $FeCl_3$: Raman Determination of Fermi Level, Layer by Layer Decoupling, and Stability. *J. Am. Chem. Soc.* **2011**, *133*, 5941–5946.
12. Zhao, W. J.; Tan, P. H.; Zhang, J.; Liu, J. A. Charge Transfer and Optical Phonon Mixing in Few-Layer Graphene Chemically Doped with Sulfuric Acid. *Phys. Rev. B* **2010**, 82.
13. Jung, N.; Kim, N.; Jockusch, S.; Turro, N. J.; Kim, P.; Brus, L. Charge Transfer Chemical Doping of Few Layer Graphenes: Charge Distribution and Band Gap Formation. *Nano Lett.* **2009**, *9*, 4133–4137.
14. Jung, N.; Crowther, A. C.; Kim, N.; Kim, P.; Brus, L. Raman Enhancement on Graphene: Adsorbed and Intercalated Molecular Species. *ACS Nano* **2010**, *4*, 7005–7013.
15. Blake, P.; Hill, E. W.; Neto, A. H. C.; Novoselov, K. S.; Jiang, D.; Yang, R.; Booth, T. J.; Geim, A. K. Making Graphene Visible. *Appl. Phys. Lett.* **2007**, 91.
16. Casiraghi, C.; Hartschuh, A.; Lidorikis, E.; Qian, H.; Harutyunyan, H.; Gokus, T.; Novoselov, K. S.; Ferrari, A. C. Rayleigh Imaging of Graphene and Graphene Layers. *Nano Lett.* **2007**, *7*, 2711–2717.
17. Nair, R. R.; Blake, P.; Grigorenko, A. N.; Novoselov, K. S.; Booth, T. J.; Stauber, T.; Peres, N. M. R.; Geim, A. K. Fine Structure Constant Defines Visual Transparency of Graphene. *Science* **2008**, *320*, 1308–1308.
18. Bruna, M.; Borini, S. Optical Constants of Graphene Layers in the Visible Range. *Appl. Phys. Lett.* **2009**, 94.
19. Mak, K. F.; Sfeir, M. Y.; Wu, Y.; Lui, C. H.; Misewich, J. A.; Heinz, T. F. Measurement of the Optical Conductivity of Graphene. *Phys. Rev. Lett.* **2008**, *101*, 196405.
20. Guerard, D.; Foley, G. M. T.; Zanini, M.; Fischer, J. E. Electronic-Structure of Donor-Type Graphite Intercalation Compounds. *Nuovo Cimento Soc. Ital. Fis., B* **1977**, *38*, 410–417.
21. Yang, M. H.; Eklund, P. C. Optical Dielectric Function of High-Stage Potassium Graphite-Intercalation Compounds—Experiment and Theory. *Phys. Rev. B* **1988**, *38*, 3505–3516.
22. Mak, K. F.; Sfeir, M. Y.; Wu, Y.; Lui, C. H.; Misewich, J. A.; Heinz, T. F. Measurement of the Optical Conductivity of Graphene. *Phys. Rev. Lett.* **2008**, *101*, 196405.
23. Boeri, L.; Bachelet, G. B.; Giantomassi, M.; Andersen, O. K. Electron-Phonon Interaction in Graphite Intercalation Compounds. *Phys. Rev. B* **2007**, 76.
24. Eklund, P. C.; Dresselhaus, G.; Dresselhaus, M. S.; Fischer, J. E. Raman-Scattering from in-Plane Lattice Modes in Low-Stage Graphite-Alkali-Metal Compounds. *Phys. Rev. B* **1977**, *16*, 3330–3333.
25. Eklund, P. C.; Subbaswamy, K. R. Analysis of Breit–Wigner Line-Shapes in the Raman-Spectra of Graphite-Intercalation Compounds. *Phys. Rev. B* **1979**, *20*, 5157–5161.
26. Nemanich, R. J.; Solin, S. A.; Guerard, D. Raman-Scattering from Intercalated Donor Compounds of Graphite. *Phys. Rev. B* **1977**, *16*, 2665–2672.
27. Brown, S. D. M.; Jorio, A.; Corio, P.; Dresselhaus, M. S.; Dresselhaus, G.; Saito, R.; Kneipp, K. Origin of the Breit–Wigner–Fano Lineshape of the Tangential G-Band Feature of Metallic Carbon Nanotubes. *Phys. Rev. B* **2001**, 63.
28. Nguyen, K. T.; Gaur, A.; Shim, M. Fano Lineshape and Phonon Softening in Single Isolated Metallic Carbon Nanotubes. *Phys. Rev. Lett.* **2007**, 98.
29. Chen, G.; Furtado, C. A.; Kim, U. J.; Eklund, P. C. Alkali-Metal-Doping Dynamics and Anomalous Lattice Contraction of Individual Debundled Carbon Nanotubes. *Phys. Rev. B* **2005**, 72.

30. Calandra, M.; Mauri, F. Theoretical Explanation of Superconductivity in C_6Ca. *Phys. Rev. Lett.* **2005**, *95*, 237002.
31. Timp, G.; Elman, B. S.; Al-Jishi, R.; Dresselhaus, G. Observation of Superlattice-Induced Raman Modes in Graphite–Potassium–Amalgam Compounds. *Solid State Commun.* **1982**, *44*, 987–991.
32. Caragiu, M.; Finberg, S. Alkali Metal Adsorption on Graphite: A Review. *J. Phys.: Condens. Matter* **2005**, *17*, R995–R1024.
33. Horie, C.; Maeda, M.; Kuramoto, Y. Lattice Dynamics of First-Stage Alkali Metal Graphite Intercalation Compounds. *Phys. B, C (Amsterdam)* **1980**, *99*, 430–434.
34. Howard, C. Tunable Nonadiabatic Renormalization of the Phonons in Heavily Doped Graphene. *arXiv.org, e-Print Archive, Condens. Matter* **2010**, *1*, 0.
35. Rousseaux, F.; Moret, R.; Guerard, D.; Lagrange, P. X-ray Study of the Liquid and Solid Phases of the Alkali Metals in KC_{24} and RbC_{24}-Intercalated Graphite Single Crystals. *Phys. Rev. B* **1990**, *42*, 725.
36. Senbetu, L.; Ikezi, H. Band Model for the Electronic-Structure of $KHgC_8$. *Phys. Rev. B* **1985**, *32*, 750–754.
37. Rytkönen, K.; Akola, J.; Manninen, M. Density Functional Study of Alkali-Metal Atoms and Monolayers on Graphite (0001). *Phys. Rev. B* **2007**, *75*, 075401.
38. Inoshita, T.; Nakao, K.; Kamimura, H. Electronic-Structure of Potassium-Graphite Intercalation Compound—C_8K. *J. Phys. Soc. Jpn.* **1977**, *43*, 1237–1243.
39. Tsuzuku, T. Anisotropic Electrical Conduction in Relation to the Stacking Disorder in Graphite. *Carbon* **1979**, *17*, 293–299.
40. Murray, J. J.; Ubbelohde, A. R. Electronic Properties of Some Synthetic Metals Derived from Graphite. *Proc. R. Soc. London Ser. A* **1969**, *312*, 371.
41. Eklund, P. C.; Mahan, G. D.; Spolar, J. G.; Arakawa, E. T.; Zhang, J. M.; Hoffman, D. M. Resonant Interband Raman Scattering in Metals and Semimetals. *Solid State Commun.* **1986**, *57*, 567–570.
42. Ohana, I.; Yacoby, Y.; Schmeltzer, D. Raman Scattering on Stage 1 C/Asf5—Coupled Electron-Phonon Excitation. *Solid State Commun.* **1986**, *60*, 839–841.
43. Ohana, I.; Dresselhaus, M. S.; Tanuma, S. Resonant Raman Effect and Fano Distortion in the Stage-2 Graphite Donor Intercalation Compound C/Rb. *Phys. Rev. B* **1991**, *43*, 1773.